Spatial Total RNA Sequencing of Formalin-Fixed Paraffin Embedded Tissues by spRandom-seq

Yuan Liao,[+][a] Jiaye Chen,[+][a] Shunji Zhang,[+][b] Yu-sheng Chen, [a] Yuexiao Lyu, [a] Bin Zhu, [c] Haide Chen, [a] Yuyi Zhu, [c] Ziye Xu, [a] Yafei Yin, [d] Xushen Xiong, [a] Nan Liu, [a] Hongshan Guo, [a] Yongcheng Wang*[a] [b]

---

[a] Dr. Y. Liao, Mr. J. Chen, Dr. Y. Chen, Miss Y. Lyu, Dr. H. Chen, Dr. Z. Xu, Prof. X. Xiong, Prof. N. Liu, Pro. H. Guo, Prof. Y. Wang
Department of Laboratory Medicine of The First Affiliated Hospital & Liangzhu Laboratory, Zhejiang University School of Medicine
Zhejiang University
Hangzhou 310030, China
E-mail: yongcheng@zju.edu.cn

[b] Mr. S. Zhang, Prof. Y. Wang
College of Biomedical Engineering and Instrument Science
Zhejiang University
Hangzhou 310030, China

[c] Mr B. Zhu, Mrs Y. Zhu
M20 Genomics
Hangzhou 310000, China

[d] Pro. Y. Yin
Department of Cell Biology and Department of Cardiology of the Second Affiliated Hospital, Zhejiang University School of Medicine
Zhejiang University
Hangzhou 310058, China.

[+] These authors contributed equally to this work

Abstract: Current sequencing-based spatial transcriptomic methods have been widely used to resolve gene expression; however, these methods are limited to fresh or fresh-frozen samples due to the low efficiency of oligo(dT) primers in capturing RNA transcripts in degraded samples. Here, we have developed a random primer-based spatial total RNA sequencing (spRandom-seq) technology for capturing full-length total RNAs in partially degraded (low RIN values) formalin-fixed paraffin-embedded (FFPE) tissues. Our spRandom-seq approach exhibited no discernible biases at the 3'- or 5'-ends within gene bodies and could be integrated with the commercially available 10X Visium and other well-established sequencing-based spatial transcriptomic platforms. Our spRandom-seq approach outperformed oligo(dT)-based 10X Visium with an 8-fold higher capturing rate for long-non-coding RNA (lncRNA) and other non-polyadenylated RNA biotypes, including miRNA, snRNA, and miscRNA. The unsupervised clustering with solely non-coding RNAs (ncRNAs) resulted in region-specific clusters aligned perfectly with mouse brain anatomic regions. Furthermore, in the clinical FFPE sections of breast cancer, our study revealed distinct expression patterns of *MUCL1* and *JCHAIN* within the tumor region, highlighting the inherent heterogeneity. spRandom-seq provided a potential spatial method for clinical FFPE specimens with well-established and commercially available spatial platforms, ensuring ease of operation and commercial scalability for large-scale applications.

Introduction

Patients' formalin-fixed paraffin-embedded (FFPE) tissues are invaluable clinical history and follow-up information repositories. However, the total RNAs within FFPE samples are prone to fragmentation during the paraffin-embedding process and may undergo further degradation, which leads to a lack of poly-A tails, restricting the utility of oligo-dT primed reverse transcription.

Current spatially resolved transcriptomics techniques have two major categories: image-based and sequencing-based. Image-based methods such as MERFISH[1] and seqFISH+[2] have been widely applied to FFPE samples, but their targeted probes still limit them and lack full-length gene coverage. The sequencing-based methods predominantly rely on 3'-end poly(A) tails of mRNA, primarily applicable to fresh or fresh-frozen samples due to the limited success of oligo(dT) primers in degraded RNA samples.[3] Alternatively, 10X Visium Spatial Gene Expression (HD and V2 Version) could be applied to FFPE samples but still in a targeted manner. The heat-induced decrosslinking method based on oligo(dT) mRNA capture is performed for FFPE samples but is still constrained by the degradation of RNA.[4] To mitigate the lack of poly(A) tails, a process known as RNA polyadenylation was employed in a single-cell RNA sequencing method called VASA-seq which is capable of capturing full-length whole transcriptome on fresh frozen samples.[5] However, VASA-seq has not yet been validated for use with FFPE tissues and is a scRNA-seq technology lacking tissue architecture information. Recently, a novel spatial transcriptomics method, Patho-DBiT has been applied to FFPE samples using *in situ* RNA polyadenylation, and high-sensitivity transcriptomic mapping of clinical FFPE sections is achieved.[6] However, the Patho-DBiT relies on intricate microfluidic chips, presenting a challenge for widespread adoption.

Random primers can bind to any location on RNA transcripts, regardless of poly-A tails, offering an alternative strategy for total RNA sequencing and FFPE samples. Here, we introduce a random primer-based spatial total RNA sequencing method (spRandom-seq), which enables comprehensive profiling of full-length total RNA based on our previously developed random primer-based single-nucleus RNA sequencing technology (snRandom-seq).[7] The spRandom-seq captures long non-coding RNAs (lncRNAs), nascent RNAs, and other transcripts often neglected by conventional workflows.

The spRandom-seq also demonstrates uniform distribution across gene bodies when applied to clinically archived FFPE tissue specimens. Compared with Patho-DBiT, the spRandom-seq has a more even distribution across gene bodies due to equitable binding of random primers to transcripts. With mouse and clinical FFPE samples, we demonstrated that spRandom-seq can seamlessly integrate with the commercially available 10X Visium and other well-established sequencing-based spatial transcriptomics platforms with various resolutions. Furthermore, we characterized the spatial distribution of transcriptomic signatures in the FFPE mouse brain by profiling protein-coding RNAs and non-coding RNAs separately; notably, non-coding RNAs also exhibited region-specific patterns. We also conducted spatial exploration of RNA biology in archival clinical FFPE breast cancer sections, elucidating its architectural features and identifying several potential non-coding RNAs implicated in tumorigenesis. This approach allows for a deeper understanding of high-sensitivity transcriptomics and the analysis of full-length total RNA within archival clinical FFPE tissues.

Results and Discussion

Overview of the spRandom-seq Method for FFPE Tissues

The main workflow of spRandom-seq is shown in Figure 1. Initially, 5 μm sections of banked FFPE tissue blocks were cut and subjected to deparaffinization, rehydration, and decrosslinking using standard xylene, alcohol wash, and TE buffer protocols (see methods). *In situ* blocking primers were employed to extend bare single-strand DNA to avoid contamination from genomic DNA. Subsequently, total RNA was converted into cDNA through multiple annealing of random primers and oligo(dT) primers during in situ reverse transcription. The different length of random primers was evaluated using bulk test, and the results indicated no significant difference (Figure S1). The 3' hydroxyl terminus of the cDNAs was terminated with poly(dA) tails by terminal transferase (TdT). These cDNAs with poly(dA) tails were released from the section via RNA degradation and bound to poly(dT) primers immobilized on a spatial DNA barcoded slide using 10X Genomics CytAssist. The single-strand cDNAs were extended on the expression slide with a specific spatial barcode. Finally, barcoded cDNAs underwent denaturation, amplification, and preparation for paired-end sequencing using next-generation sequencing (NGS). Inevitably, the use of random primers will capture rRNA. To reduce the waste of sequencing reads and optimize the workflow of spRandom-seq, we performed rRNA depletion on two FFPE samples with the CRISPR-based strategy we employed in our previous work (Figure S2) [8]. The rRNA-depletion treatment reduced the rRNA proportion from 46.1% to 20.7% and 41.3% to 16.4% in two independent sections, respectively. In addition, the more details of spRandom-seq can be found in the Supporting Information.

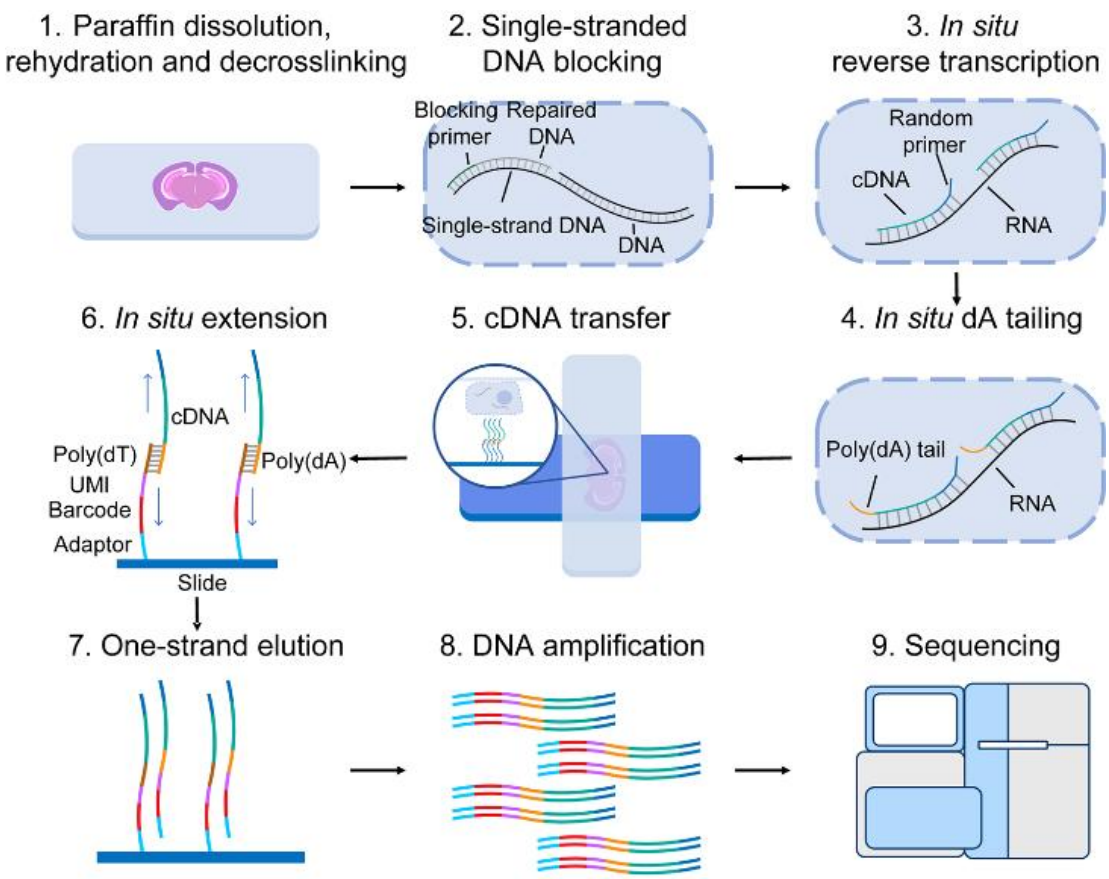

Figure 1. Overview of spRandom-seq workflow for FFPE tissues. The workflow of spRandom-seq for FFPE tissues includes FFPE section pre-treatment, single-stranded DNA blocking, reverse transcription, dA tailing, cDNA transfer, extension, one-strand elution, DNA amplification and sequencing.

Validation of spRandom-seq Using the Degraded FFPE Mouse Tissues

To evaluate the performance and versatility of this technology, we applied spRandom-seq on FFPE sections of mouse coronal brain and heart with 10X Visium slides (Resolution: 55 μm) for spatial labeling. In order to better resemble clinical samples, we selected mouse coronal brain and heart samples with severe RNA degradation (low RIN values, about 3, Figure S2). The unsupervised clustering results of our spRandom-seq data were perfectly aligned with different mouse brain anatomic regions, including cortex and subcortical regions such as hippocampus, thalamus, and striatum that were annotated with the Allen Brain Atlas based on the H&E staining (Figure 2a). We also observed reasonable corresponding pattern between the unsupervised clustering of the mouse heart section and its H&E staining, showing the robustness of our methods (Figure 2a and Figure S3). Concerning gene detection sensitivity, at the average sequencing depth of ~90,000 raw reads per single nucleus, we detected a median of 6,633 UMIs and 2,360 genes for mouse brain and 9,808 UMIs and 2,549 genes for mouse heart (Figure 2b). Different cell types were deconvoluted by CARD,[9] an NMF-based bioinformatic algorithm, with a validated single-cell RNA-seq dataset from the same tissue as reference (Figure 2c and 2d).[10] The location of each major cell type in spatial location was visualized in Figure 2c and Figure S4. For instance, the excitatory neurons specifically expressed the classical cell-type marker gene *Slc17a6* (Figure 2e). The location of these specific marker genes captured by spRandom-seq was consistent with *in situ* hybridization data from Allen Brain Atlas (Figure 2e).[11] SpRandom-seq further exhibited robust detection

capabilities for various non-coding RNAs (ncRNAs) such as *Mir6236* and *Rnu12*, which were inadequately recovered or undetectable by 10X Visium (Figure S5a and S5b). To explore the regional specificity of ncRNAs, we performed unsupervised clustering with sole ncRNAs. The spatial location of those clusters was perfectly aligned with broad mouse brain regions (Figure 2f). The major brain regions, such as the isocortex (Cluster 1), dentate gyrus (DG, Cluster 8), CA (Cluster 7 & 9), thalamus (Cluster 2), and hypothalamus (Cluster 3) were well-dissected without protein-coding features, indicating potential region-specific regulatory functions of ncRNAs (Figure 2f). We performed the differential expression analysis for each cluster with ncRNAs to further investigate the ncRNAs expressed exclusively in those brain regions (Figure S5c). Remarkably, *4921539H07Rik* exhibited the highest expression in Cluster 7 (CA1), which recapitulated the previous findings that *4921539H07Rik* is a cell-type specific lncRNA for CA1 excitatory neurons.[12] Additionally, our data showed that *4921539H07Rik* and *Neurod2* exhibited a similar spatial expression pattern in the mouse brain CA1 region (Figure 2g).[12] These data demonstrated that spRandom-seq offered an approach to spatially characterize the transcriptomic organization of intricate tissues within coding and non-coding RNAs. Moreover, to investigate the performance of spRandom-seq on other spatial transcriptomics platforms, we applied spRandom-seq on a mouse olfactory bulb FFPE section with a commercially available 15μm-resolution chip. We detected a median of 3,700 UMIs and 941 genes. The clustering results successfully aligned with the anatomic structure of mouse olfactory bulb (Figure 2h). These data indicated spRandom-seq's high compatibility with various spatial transcriptomics platforms and expression chips with different resolutions."

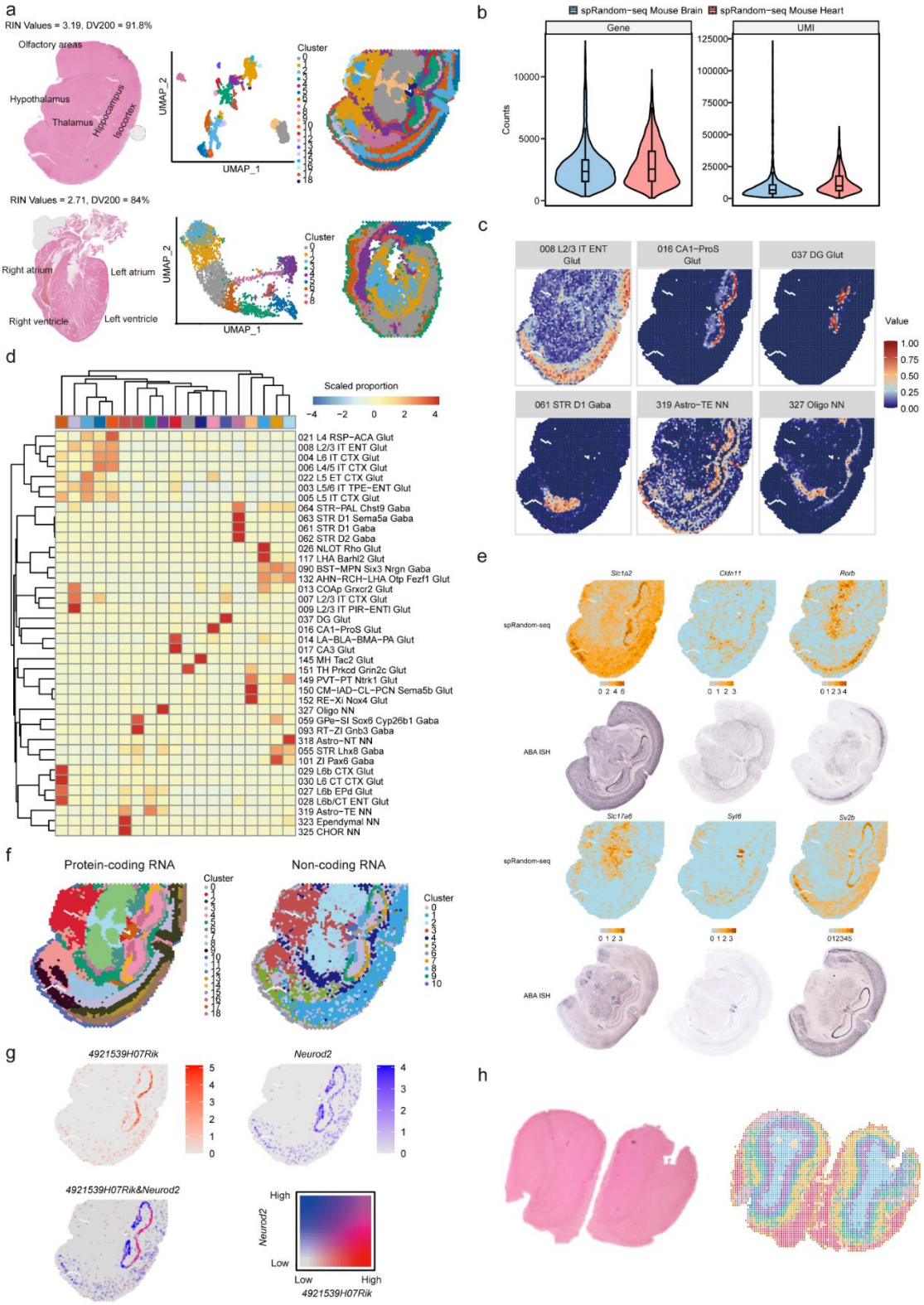

Figure 2. Validation and benchmark of spRandom-seq using a FFPE mouse brain section. a, Spatial visualization of coronal FFPE mouse brain and heart section analyzed by spRandom-seq at 55 μm resolution. b, Numbers of Genes/UMIs detection for FFPE mouse brain and heart using spRandom-seq. c, Heatmap showing the correlation between clusters and cell types. d, Spatial maps of classic cell-type for spRandom-seq in FFPE mouse brain section. Spots in which the transcript was not detected are shown as yellow. Color scale indicates log-normalized expression. e, Spatial visualization of six selected genes expressions of the FFPE mouse brain section

and ISH images of the adult mouse brain taken from ABA. f, UMAP of clustering results of coronal FFPE mouse brain section using only protein-coding or non-coding RNAs respectively. g, Spatial maps of lncRNA *4921539H07Rik* and *Neurod2* for spRandom-seq datasets. Spots in which the transcript was identified as lncRNA are depicted in red, while those identified as *Neurod2* are depicted in blue. Spots exhibiting co-expression are represented in pink. h, Spatial visualization of FFPE mouse olfactory bulb section analyzed by spRandom-seq at 15 μm resolution.

Spatial Total Transcriptome Mapping of the Clinical Archival Breast Cancer Using spRandom-seq

spRandom-seq was also employed to elucidate the cellular heterogeneity within tumor tissues obtained from a patient diagnosed with breast cancer. With 44% sequencing saturation, we detected a median of 28,942 UMIs and 5,853 genes for breast cancer section. Unsupervised clustering revealed 9 spatial clusters aligned with histological structures (Figure 3a). The UMAP delineated distinct cell types defined by canonical markers (Figure 3b). Our approach (a median of 4,309 genes and 19,759 UMIs per pixel) exhibited superior performance compared with the 10X Visium fresh frozen sample with similar sequencing depth (Figure 3c, 3d and Table S1). In addition, spRandom-seq showed no discernible 3'- or 5'-end biases throughout the gene body, in contrast to poly(A)-based 10X fresh-frozen Visium, which displays a clear 3'-end bias when subjected to NGS (Figure 3e and Figure S5). These results suggested that our method effectively captured comprehensive full-length transcripts, highlighting the critical distinction between poly(A)-based technology and the random primer-based strategy.

We performed cell-type deconvolution to obtain the cell-type distribution across the breast cancer section. The reference adult human breast single-cell RNA-seq data was retrieved from the Kumar et al.[13] The location of each major cell type in spatial location was visualized in Figure 3f. Our data revealed a high expression of ERBB2 and ESR1 but low expression of PGR in the tumor, suggesting the presence of HER2-positive breast cancer (Figure 3g). Additionally, the tumor purity score calculated by ESTIMATE accurately identified the specific regions affected by the tumor (Figure 3h).[14] We also observed a high expression of *MUCL1* in certain tumor regions, accompanied by low-expression levels of *IGHG1* and *JCHAIN*. Previous reports have suggested that this correlation is associated with worse relapse-free survival in patients.[15] These data indicated the presence of heterogeneity within the tumor region of this breast cancer patient. The elevated expression of *CD24* (but not *CD47*) in the tumor area supports its potential as a promising target for cancer immunotherapy in ovarian and breast cancers.[16] These findings highlight the ability of spRandom-seq to capture the heterogeneity present within clinical FFPE sections of breast cancer.

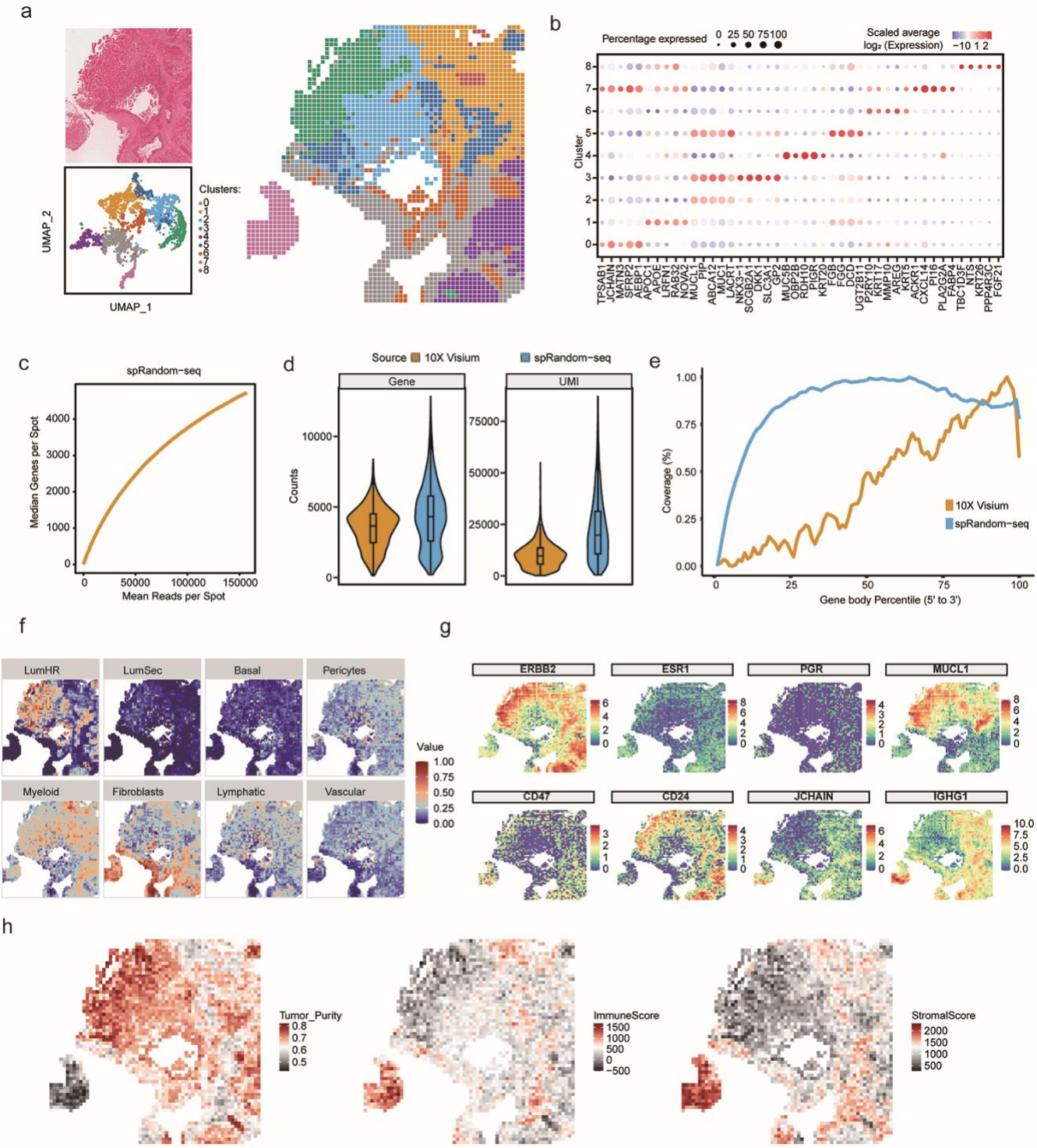

Figure 3. Validation and benchmark of spRandom-seq using a clinical FFPE breast cancer section. a, Spatial visualization of the clinical FFPE breast cancer section analyzed by spRandom-seq at 50 μm resolution. b, Dotplot of top differentially expressed genes in each cluster based on the unsupervised clustering. c, Saturation analysis of spRandom-seq based on the the clinical FFPE breast cancer tissues. d, Genes/UMIs detection comparison the clinical FFPE breast cancer tissues using spRandom-seq and fresh frozen breast by 10X Genomics. e, Read coverage along the gene body by spRandom-seq in FFPE breast cancer section. f, Cell-type deconvolution results displaying spatial distribution of major cell types in breast section. Color scale indicates the proportion of a given cell type in a spot. g, Spatial maps of classic cell-type marker genes for spRandom-seq in FFPE breast cancer section. Color scale

indicates log-normalized expression. h, Spatial maps displaying tumor purity, immune and stromal scores from ESTIMATE analysis of spRandom-seq FFPE breast cancer section.

Identification of Spatial ncRNAs in the Clinical Archival Breast Cancer Tissues

Based on random primer strategy, spRandom-seq displayed high ncRNA sensitivity. Our approach exhibited robust detection capabilities for various non-coding RNAs (ncRNAs) that were inadequately recovered or undetectable by 10X Visium, including miRNA, snRNA, lncRNA, and miscRNA (Figure 4a and 4b). To further elucidate the regulatory role of ncRNAs in tumorigenesis, we first divided the human breast cancer section into "High (Normalized value > 0.5)" and "Low (Normalized value <= 0.5)" regions according to the min-max normalized values of tumor purity, immune score, and stromal score, respectively (Figure S6a). We then conducted a differential expression (DE) analysis for ncRNAs and protein-coding genes between the high and low tumor/immune/stromal regions (Figure 4c and Figure S6b). A Pearson's correlation test was performed on each pair of significant DE ncRNAs and DE protein-coding genes. Many DE ncRNAs that showed a significant positive correlation with those region-specific protein-coding genes have been reported to be relevant. For instance, the pseudogene *CYP4Z2P* that was highly correlated with DEGs in the high tumor region has been shown to be responsible for maintaining the stemness of breast cancer cells in a previous study (Figure 4c).[17] To investigate the potential biological pathways that are associated with those up-regulated ncRNAs in those regions, GO enrichment analysis was performed on the DE protein-coding genes that showed positive correlations with the top upregulated ncRNAs in high tumor/immune/stromal regions respectively (Figure 4d and Figure S6c). These were enriched mainly in biological pathway categories associated with epithelial to mesenchymal transition and negative regulation of programmed cell death (Figure 4f).

In total, we developed a random primer-based spatial total RNA sequencing technology by capturing full-length total RNAs with random primers. spRandom-seq was developed and improved on the basis of our previous work snRandom-seq, a droplet-based single-nucleus RNA sequencing technology tailored for FFPE tissues. The snRandom-seq requires tissue dissociation followed by nucleus isolation, and the cDNA is barcoded using capture probes integrated into droplets, while spRandom-seq is a platform designed explicitly for spatial total RNA sequencing, enabling in situ decrosslinking and the precise localization of transcripts within tissue samples. The cDNA is barcoded using capture probes that are spatially indexed. This innovative approach offers a potential spatial method for analyzing clinical FFPE specimens. Notably, spRandom-seq leverages widely used spatial gene expression chips such as the popular 10X Visium platform, ensuring ease of operation and commercial scalability for large-scale applications.

Current spatially resolved transcriptomics techniques mainly rely on 3'-end poly(A) tails of mRNA, which are limited to non-degraded RNA samples. However, 10X Visium Spatial Gene Expression utilizes probe-based technology to capture spatial information for genes of interest, albeit with limited coverage of the whole transcriptome. In contrast, spRandom-seq enables unbiased and efficient spatial transcription profiling on FFPE samples. Our method also has several limitations. The resolution of the expression slides in our experiments was about 55 and 15 μm, which precluded analysis at single-cell resolution for several cell types. To achieve single-cell resolution, it is imperative to employ expression slides with higher spatial resolution in our methodology.

Additionally, the utilization of random primers in spRandom-Seq facilitates enhanced coverage of gene body regions, thereby enabling the identification of a substantial number of ncRNAs and facilitating the exploration of nascent transcripts. The availability of these comprehensive full-length total spatial RNA-seq datasets suggests the potential for a thorough analysis of copy number variation (CNV) and mutations at the spatial level.

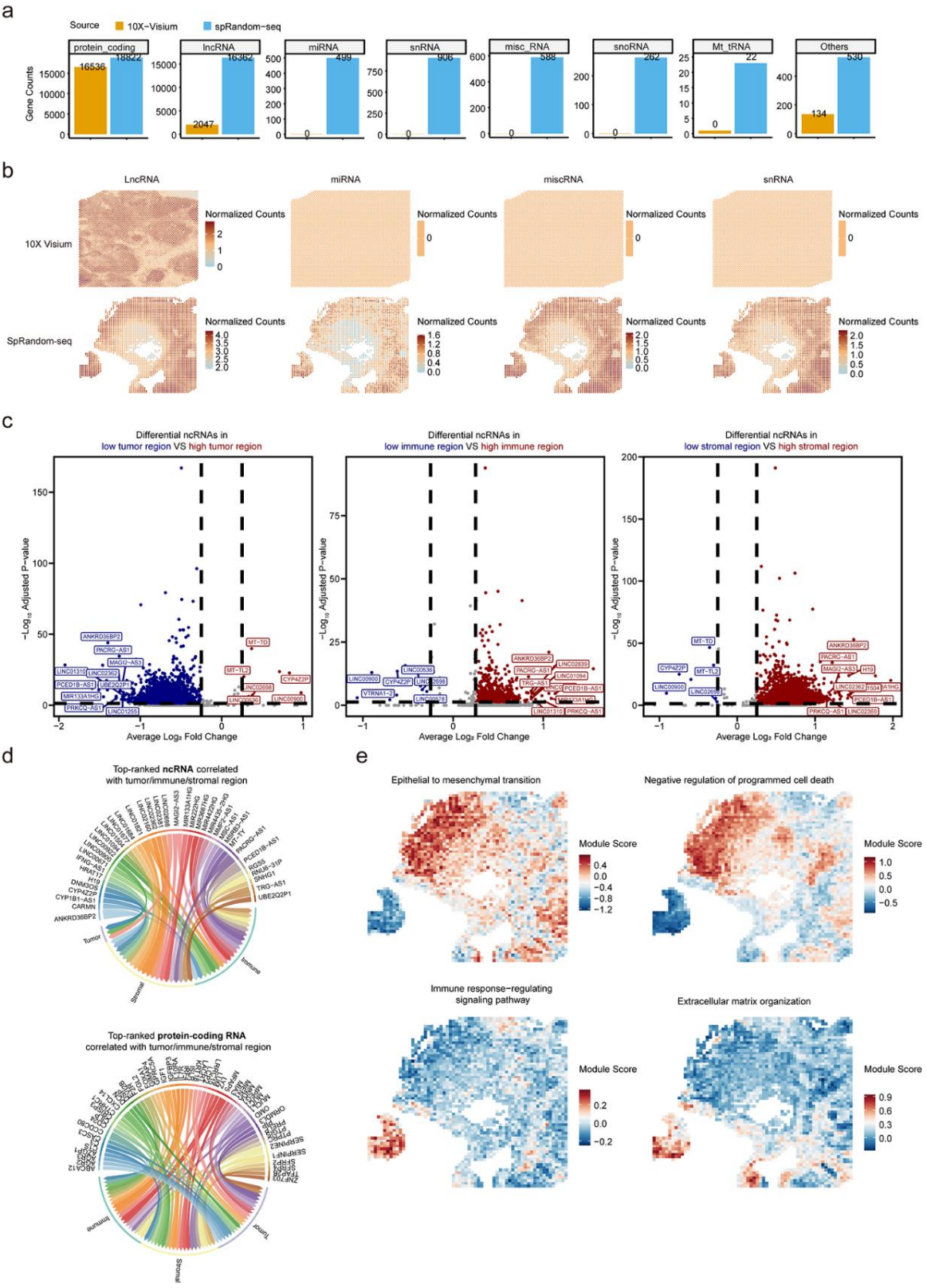

Figure 4. Spatial ncRNA regulation in the clinical FFPE breast cancer section. a, Comparison of different RNA biotypes detection between spRandom-seq FFPE breast cancer section and 10X Visium fresh frozen breast cancer section. b, Spatial count maps of various ncRNA biotypes. c, Volcano plots displaying differentially expressed ncRNAs between the high tumor/immune/stromal and low tumor/immune/stromal regions. d, Top-ranked upregulated ncRNAs and protein-coding RNAs showing high correlation with the

tumor/immune/stromal regions. e, Spatial interactions involving the top upregulated ncRNAs and upstream signaling pathways. The biological pathways were enriched by all protein coding DEGs that showed positive correlation with the ncRNAs. Module score was calculated based on the expression of all intersection genes of a given GO term.

Conclusion

spRandom-seq provided a novel approach for detecting the composition of transcriptomic signatures in mouse and clinical archival FFPE samples with protein-coding and non-coding RNAs, respectively. To our knowledge, we are the first to introduce a random primer-based spatial total RNA sequencing technology for FFPE tissues by capturing full-length total RNAs. It enabled comprehensive capture of full-length transcripts within the degraded FFPE samples and a wide range of RNA biotypes, including lncRNAs, newly transcribed RNAs, and other RNAs often overlooked by conventional spatial transcriptomics methods. Our spRandom-seq approach also exhibited no discernible biases at the 3'- or 5'-ends within gene bodies, thereby facilitating the detection of RNA variable splicing and gene mutations in spatial omics studies. Importantly, spRandom-seq leverages widely used spatial gene expression chips such as the popular 10X Visium platform, ensuring ease of operation and commercial scalability for large-scale applications.

In conclusion, the straightforward experimental protocol and comprehensive spatial transcriptomic information obtained from the FFPE tissues described in this study are anticipated to facilitate the future large-scale application of spRandom-seq in basic and clinical research endeavors.

Acknowledgements

The project was supported by "Pioneer" R&D programs of Zhejiang Province (No. 2024C03005, Y.W.), the National Natural Science Foundation of China (No. 32200073, Y.W., 32250710678, Y.W. and No. 82200977, Z.X.), Leading Innovative and Entrepreneur Team Introduction Program of Zhejiang (No. 2021R01012, Y.W.), and Key R&D Program of Zhejiang (No. 2024SSYS0022, Y.W.). Thanks for the technical support from the core facilities of Zhejiang University and Liangzhu Laboratory.

Keywords: spatial transcriptomics • random primer • full-length total transcriptomics

[1] K. H. Chen, A. N. Boettiger, J. R. Moffitt, S. Wang, X. Zhuang, *Science* **2015**, *348*.

[2] C.-H. L. Eng, M. Lawson, Q. Zhu, R. Dries, N. Koulena, Y. Takei, J. Yun, C. Cronin, C. Karp, G.-C. Yuan, L. Cai, *Nature* **2019**, *568*, 235-239.

[3] aS. G. Rodriques, R. R. Stickels, A. Goeva, C. A. Martin, E. Murray, C. R. Vanderburg, J. Welch, L. M. Chen, F. Chen, E. Z. Macosko, *Science* **2019**, *363*, 1463-1467; bC. S. Cho, J. Xi, Y. Si, S. R. Park, J. E. Hsu, M. Kim, G. Jun, H. M. Kang, J. H. Lee, *Cell* **2021**, *184*, 3559-3572 e3522; cA. Chen, S. Liao, M. Cheng, K. Ma, L. Wu, Y. Lai, X. Qiu, J. Yang, J. Xu, S. Hao, X. Wang, H. Lu, X. Chen, X. Liu, X. Huang, Z. Li, Y. Hong, Y. Jiang, J. Peng, S. Liu, M. Shen, C. Liu, Q. Li, Y. Yuan, X. Wei, H. Zheng, W. Feng, Z. Wang, Y. Liu, Z. Wang, Y. Yang, H. Xiang, L. Han, B. Qin, P. Guo, G. Lai, P. Munoz-Canoves, P. H. Maxwell, J. P. Thiery, Q. F. Wu, F. Zhao, B. Chen, M. Li, X. Dai, S. Wang, H. Kuang, J. Hui, L. Wang, J. F. Fei, O. Wang, X. Wei, H. Lu, B. Wang, S. Liu, Y. Gu, M. Ni, W. Zhang, F. Mu, Y. Yin, H. Yang, M. Lisby, R. J. Cornall, J. Mulder, M. Uhlen, M. A. Esteban, Y. Li, L. Liu, X. Xu, J. Wang, *Cell* **2022**, *185*, 1777-1792 e1721; dD. Gyllborg, C. M. Langseth, X. Qian, E. Choi, S. M. Salas, M. M. Hilscher, E. S. Lein, M. Nilsson, *Nucleic Acids Research* **2020**, *48*, e112-e112; eX. Wang, W. E.

Allen, M. A. Wright, E. L. Sylwestrak, N. Samusik, S. Vesuna, K. Evans, C. Liu, C. Ramakrishnan, J. Liu, G. P. Nolan, F.-A. Bava, K. Deisseroth, *Science* **2018**, *361*.

[4] E. Gracia Villacampa, L. Larsson, R. Mirzazadeh, L. Kvastad, A. Andersson, A. Mollbrink, G. Kokaraki, V. Monteil, N. Schultz, K. S. Appelberg, N. Montserrat, H. Zhang, J. M. Penninger, W. Miesbach, A. Mirazimi, J. Carlson, J. Lundeberg, *Cell Genomics* **2021**, *1*.

[5] F. Salmen, J. De Jonghe, T. S. Kaminski, A. Alemany, G. E. Parada, J. Verity-Legg, A. Yanagida, T. N. Kohler, N. Battich, F. van den Brekel, A. L. Ellermann, A. M. Arias, J. Nichols, M. Hemberg, F. Hollfelder, A. van Oudenaarden, *Nat Biotechnol* **2022**, *40*, 1780-1793.

[6] Z. Bai, D. Zhang, Y. Gao, B. Tao, D. Zhang, S. Bao, A. Enninful, Y. Wang, H. Li, G. Su, X. Tian, N. Zhang, Y. Xiao, Y. Liu, M. Gerstein, M. Li, Y. Xing, J. Lu, M. L. Xu, R. Fan, *Cell* **2024**.

[7] Z. Xu, T. Zhang, H. Chen, Y. Zhu, Y. Lv, S. Zhang, J. Chen, H. Chen, L. Yang, W. Jiang, S. Ni, F. Lu, Z. Wang, H. Yang, L. Dong, F. Chen, H. Zhang, Y. Chen, J. Liu, D. Zhang, L. Fan, G. Guo, Y. Wang, *Nature Communications* **2023**, *14*.

[8] Z. Xu, Y. Wang, K. Sheng, R. Rosenthal, N. Liu, X. Hua, T. Zhang, J. Chen, M. Song, Y. Lv, S. Zhang, Y. Huang, Z. Wang, T. Cao, Y. Shen, Y. Jiang, Y. Yu, Y. Chen, G. Guo, P. Yin, D. A. Weitz, Y. Wang, *Nature Communications* **2023**, *14*.

[9] Y. Ma, X. Zhou, *Nature Biotechnology* **2022**, *40*, 1349-1359.

[10] Z. Yao, C. T. J. van Velthoven, M. Kunst, M. Zhang, D. McMillen, C. Lee, W. Jung, J. Goldy, A. Abdelhak, M. Aitken, K. Baker, P. Baker, E. Barkan, D. Bertagnolli, A. Bhandiwad, C. Bielstein, P. Bishwakarma, J. Campos, D. Carey, T. Casper, A. B. Chakka, R. Chakrabarty, S. Chavan, M. Chen, M. Clark, J. Close, K. Crichton, S. Daniel, P. DiValentin, T. Dolbeare, L. Ellingwood, E. Fiabane, T. Fliss, J. Gee, J. Gerstenberger, A. Glandon, J. Gloe, J. Gould, J. Gray, N. Guilford, J. Guzman, D. Hirschstein, W. Ho, M. Hooper, M. Huang, M. Hupp, K. Jin, M. Kroll, K. Lathia, A. Leon, S. Li, B. Long, Z. Madigan, J. Malloy, J. Malone, Z. Maltzer, N. Martin, R. McCue, R. McGinty, N. Mei, J. Melchor, E. Meyerdierks, T. Mollenkopf, S. Moonsman, T. N. Nguyen, S. Otto, T. Pham, C. Rimorin, A. Ruiz, R. Sanchez, L. Sawyer, N. Shapovalova, N. Shepard, C. Slaughterbeck, J. Sulc, M. Tieu, A. Torkelson, H. Tung, N. Valera Cuevas, S. Vance, K. Wadhwani, K. Ward, B. Levi, C. Farrell, R. Young, B. Staats, M.-Q. M. Wang, C. L. Thompson, S. Mufti, C. M. Pagan, L. Kruse, N. Dee, S. M. Sunkin, L. Esposito, M. J. Hawrylycz, J. Waters, L. Ng, K. Smith, B. Tasic, X. Zhuang, et al., *Nature* **2023**, *624*, 317-332.

[11] E. S. Lein, M. J. Hawrylycz, N. Ao, M. Ayres, A. Bensinger, A. Bernard, A. F. Boe, M. S. Boguski, K. S. Brockway, E. J. Byrnes, L. Chen, L. Chen, T. M. Chen, M. C. Chin, J. Chong, B. E. Crook, A. Czaplinska, C. N. Dang, S. Datta, N. R. Dee, A. L. Desaki, T. Desta, E. Diep, T. A. Dolbeare, M. J. Donelan, H. W. Dong, J. G. Dougherty, B. J. Duncan, A. J. Ebbert, G. Eichele, L. K. Estin, C. Faber, B. A. Facer, R. Fields, S. R. Fischer, T. P. Fliss, C. Frensley, S. N. Gates, K. J. Glattfelder, K. R. Halverson, M. R. Hart, J. G. Hohmann, M. P. Howell, D. P. Jeung, R. A. Johnson, P. T. Karr, R. Kawal, J. M. Kidney, R. H. Knapik, C. L. Kuan, J. H. Lake, A. R. Laramee, K. D. Larsen, C. Lau, T. A. Lemon, A. J. Liang, Y. Liu, L. T. Luong, J. Michaels, J. J. Morgan, R. J. Morgan, M. T. Mortrud, N. F. Mosqueda, L. L. Ng, R. Ng, G. J. Orta, C. C. Overly, T. H. Pak, S. E. Parry, S. D. Pathak, O. C. Pearson, R. B. Puchalski, Z. L. Riley, H. R. Rockett, S. A. Rowland, J. J. Royall, M. J. Ruiz, N. R. Sarno, K. Schaffnit, N. V. Shapovalova, T. Sivisay, C. R. Slaughterbeck, S. C. Smith, K. A. Smith, B. I. Smith, A. J. Sodt, N. N. Stewart, K. R. Stumpf, S. M. Sunkin, M. Sutram, A. Tam, C. D. Teemer, C. Thaller, C. L. Thompson, L. R. Varnam, A. Visel, R. M. Whitlock, P. E. Wohnoutka, C. K. Wolkey, V. Y. Wong, et al., *Nature* **2007**, *445*, 168-176.

[12] M. Niu, W. Cao, Y. Wang, Q. Zhu, J. Luo, B. Wang, H. Zheng, D. A. Weitz, C. Zong, *Nat Biotechnol* **2023**.

[13] T. Kumar, K. Nee, R. Wei, S. He, Q. H. Nguyen, S. Bai, K. Blake, M. Pein, Y. Gong, E. Sei, M. Hu, A. K. Casasent, A. Thennavan, J. Li, T. Tran, K. Chen, B. Nilges, N. Kashikar, O. Braubach, B. Ben Cheikh, N. Nikulina, H. Chen, M. Teshome, B. Menegaz, H. Javaid, C. Nagi, J. Montalvan, T. Lev, S. Mallya, D. F. Tifrea, R. Edwards, E. Lin, R. Parajuli, S. Hanson, S. Winocour, A. Thompson, B. Lim, D. A. Lawson, K. Kessenbrock, N. Navin, *Nature* **2023**, *620*, 181-191.

[14] K. Yoshihara, M. Shahmoradgoli, E. Martínez, R. Vegesna, H. Kim, W. Torres-Garcia, V. Treviño, H. Shen, P. W. Laird, D. A. Levine, S. L. Carter, G. Getz, K. Stemke-Hale, G. B. Mills, R. G. Verhaak, *Nat Commun* **2013**, *4*, 2612.

[15] L. Jia, Y. Ling, K. Li, L. Zhang, Y. Wang, H. Kang, *Clin Breast Cancer* **2021**, *21*, e654-e664.

[16] A. A. Barkal, R. E. Brewer, M. Markovic, M. Kowarsky, S. A. Barkal, B. W. Zaro, V. Krishnan, J. Hatakeyama, O. Dorigo, L. J. Barkal, I. L. Weissman, *Nature* **2019**, *572*, 392-396.

[17] L. Zheng, Q. Guo, C. Xiang, S. Liu, Y. Jiang, L. Gao, H. Ni, T. Wang, Q. Zhao, H. Liu, Y. Xing, Y. Wang, X. Li, T. Xi, *J Hematol Oncol* **2019**, *12*, 23.

[18] A. Kozomara, M. Birgaoanu, S. Griffiths-Jones, *Nucleic Acids Res* **2019**, *47*, D155-d162.

Entry for the Table of Contents

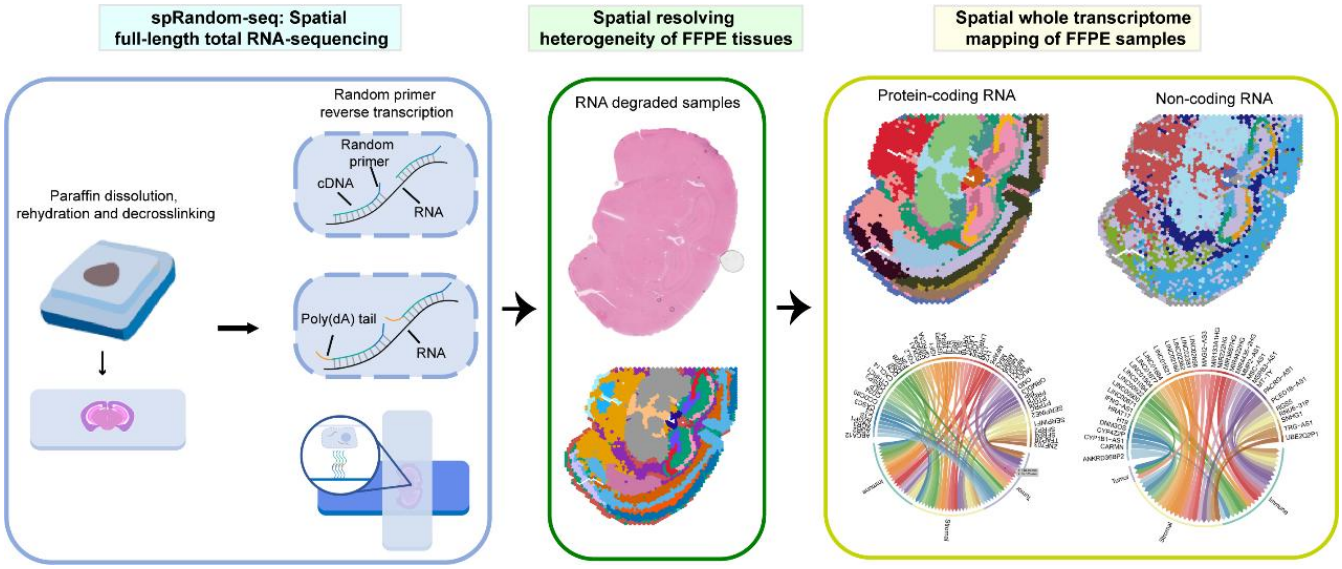

spRandom-seq could be the first to introduce a random primer-based spatial total RNA sequencing technology for FFPE tissues.

It enabled capture of full-length transcripts within the degraded FFPE samples and undetectable RNA biotypes compared with oligo(dT)-based methods, including miRNA, snRNA, and miscRNA.

It provided a potential spatial method for clinical FFPE specimens with well-established and commercially available spatial platfo